

Effect of nozzle-to-plate spacing on the development of a plane jet impinging on a heated plate

Ben Kalifa Rim¹ · Nejla Mahjoub Saïd² · Hervé Bournot³ · Georges Le Palec³

Received: 12 September 2015 / Accepted: 25 August 2016 / Published online: 1 September 2016
© Springer-Verlag Berlin Heidelberg 2016

Abstract An experimental investigation was carried out to study the behavior of a turbulent air jet impinging on a heated plate. The study of the flow field was performed using a particle image velocimetry. A three-dimensional numerical model with Reynolds stress model has been conducted to examine the global flow. Numerical results agree well with experimental data. The main properties of the fluid occurring between the nozzle and the flat plate are presented. In addition, the effect of the distance between the nozzle exit and the plate ($h/e = 14$ and 28) were investigated and detailed analysis of the dynamic, turbulent distribution and temperature fields were performed. The wall shear stress and the pressure fields near the heated plate are then explored. Results showed that the mean velocity and the heat transfer characteristics of small nozzle-to-plate spacing are significantly different from those of large nozzle-to-plate spacing.

1 Introduction

Impinging jets have received considerable attention due to their inherent characteristics of high rates of heat transfer. Such impinging flow devices allow for short flow paths and relatively high rates of cooling from comparatively small

surface area. Impinging jets are encountered in wide range applications. Major industrial applications of impinging jets include heating, cooling, and drying of food products, textiles, papers, processing of some metals and glass, cooling of gas turbine blades and the outer walls of combustion chambers, cooling of electronic equipment, etc. Due to this diverse range of applications, significant attention has been paid to impinging jets. Many investigations of the heat transfer characteristics of impinging jets have been performed in the past decades [1–9]. Heat transfer rates in case of impinging jets are influenced by parameters such as Reynolds number, jet-to-plate spacing, radial distance from stagnation point, confinement of the jet, nozzle geometry, curvature of the target plate, roughness of the target plate and turbulence intensity at the nozzle exit.

The impingement of a jet on a solid surface has a scientific interest due to the presence of different flow regimes. The flow field of an impinging jet divided into three regions [10]. Firstly there is the free jet zone, which is the region that is largely unaffected by the presence of the impingement surface. This region can also be divided into two sub-regions: the zone of flow development is where the core of the jet still persists and centerline velocities are thus constant. Secondary, there is a stagnation zone that extends to a radial location defined by the spread of the jet. The stagnation zone includes the stagnation point where the mean velocity is zero. Finally, the wall jet zone extends beyond the radial limits of the stagnation zone.

The configuration of a plane jet impinging normally on a flat plate has been studied most by several authors. Gutmark et al. [11] examined an experimental study of the turbulent structures of a two-dimensional impinging jet. The mean velocity, turbulent stresses are measured and the energy balances for the three fluctuating components are calculated. They found that velocity varies linearly in the

✉ Nejla Mahjoub Saïd
nejla.mahjoub@fsm.rnu.tn

¹ LGM, National Engineering School of Monastir, University of Monastir, Monastir, Tunisia

² LGM, ENIM, Preparatory Institute for Engineering Studies, University of Monastir, Monastir, Tunisia

³ IUSTI, UMR 7343, Faculty of Sciences, University of Aix-Marseille, Marseille, France

immediate vicinity of the plate. The jet is not affected by the presence of the plate over 75 % of the distance between the nozzle and the plate.

The behavior of a three-dimensional impinging jet has been reported by Cooper et al. [12], Knowles and Myszko [13] and O'Donovan and Murray [14]. Actually, Cooper et al. [12] report an extensive set of measurements of a turbulent jet impinging orthogonally onto a large plane surface. Two Reynolds numbers were been considered, $2.3 \cdot 10^4$ and $7 \cdot 10^4$, while the height of the jet discharge above the plate ranges from two to ten diameters, with particular attention focused on two and six diameters. The experiment has been designed so that it provides hydrodynamic data for conditions the same as those for which Baughn and Shimizu [15].

Knowles and Myszko [13] reported an experimental study of a circular jet impinging onto a flat ground board. The nozzle to ground board separation (h) varying between 2 and 10 diameters (d). Measurements were performed in the free and wall-jets using cross-wire hotwire anemometry, mean velocity, normal and shear stress results being presented. Nozzle height was found to affect the initial thickness of the wall-jet leaving the impingement region, increasing h/d increasing the wall-jet thickness.

O'Donovan and Murray [14] presented experimental results of fluid flow and heat transfer relating to an axially symmetric impinging air jet. It has been shown that at low nozzle to impingement surface spacing the mean heat transfer distribution in the radial direction exhibits secondary peaks. These peaks have been reported by several investigators and have been attributed, in general, to an abrupt increase in turbulence in the wall jet boundary layer.

Many investigations have been carried out to illustrate the effect of parameters where they affect the evolution of the turbulent impinging jets. Flow structures of impinging jets are influenced by factors, such as nozzle-to-plate spacing (h/e) [16–18], Reynolds number (Re) [19] and the temperature of the flat surface [20–22], which have been examined both experimentally and numerically.

An experimental study of flow field is conducted by Narayanan et al. [16] for two nozzle-to-surface spacing (3.5 and 0.5 nozzle exit hydraulic diameters). Fluid mechanical data include measurements of the mean flow field and variance of normal and cross velocity fluctuations, mean surface pressure, and RMS surface pressure fluctuations along the nozzle minor axis. The fluid flow results indicate that past impingement, locations of high streamwise fluctuating velocity variance occur in the wall jet flow for both nozzle spacing. Their work provides an insight into the distinctly different flow field and heat transport mechanisms that occur during impingement of the jet transitional and potential-core regions.

The flow field of confined circular and elliptic jets was studied experimentally by Koseoglu and Baskaya [17] with a laser Doppler anemometry (LDA) In addition, heat transfer characteristics were numerically investigated. Experiments were conducted with a circular jet and an elliptic jet, jet to target spacing of 2 and 6 jet diameters, and Reynolds number 10,000. Differences between the circular and elliptic jet, in terms of flow field and heat transfer characteristics, reduced with increase in the jet to plate distance.

Also Ben Kalifa et al. [18] have experimentally investigated the flow and the heat transfer characteristics of a round air jet using Particle Image Velocimetry (PIV) technique. The effect of the nozzle distance ($h/d = 1$ and 2) on the dynamic characteristics and the turbulence behavior is determined. For a fixed Reynolds number, the influence of the distance between the nozzle exit and the flat plate on the stagnation point is well captured. The authors found that when the distance increases, the separation point approaches to the jet axis. In addition, the results indicated that the potential core length is found depending on the nozzle-to-surface spacing (h/d).

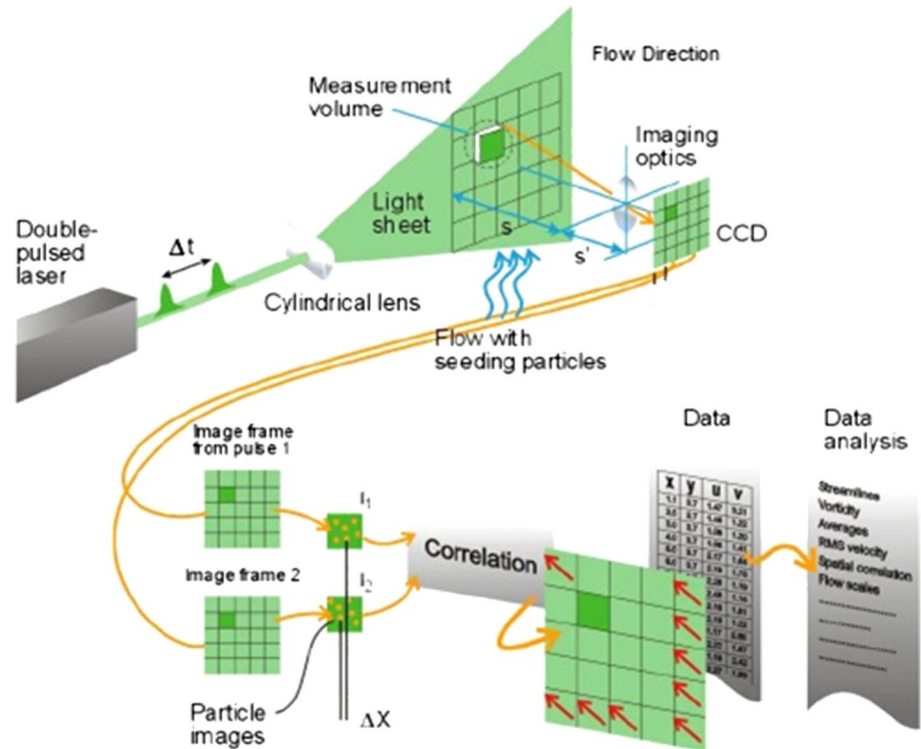
The sensitivity of the orthonormal impinging jets with respect to scale (Reynolds number), boundary conditions (geometry and surface roughness) as well as inlet conditions is investigated by Hangan [19]. They show that the flow is only weakly dependent on the distance between the jet and the surface for distances larger than the ring-vortex formation length. Radial confinements of diameters less than approximately 10 jet diameters and axial confinements placed at less than one jet diameter above the surface affect the pressure distribution on the impinging plate.

The flow field of plane impinging jets at moderate Reynolds numbers has been computed by Beaubert and Viazzo [20] a using large eddy simulation technique. Two Reynolds numbers ($Re = 3000$ and 7500) defined by the jet exit conditions are considered. The simulations were performed to study the mean velocity, the turbulence statistics along the jet axis and at different vertical locations. The effect of the jet Reynolds number is significant between 3000 and 7500 both on the near and far field structure.

The experiments carried out by Guerra et al. [21] were conducted for one nozzle to-plate spacing ($h/d = 2$) and Reynolds number of 35,000. A constant wall heat flux was achieved by means of a resistance heater place in close contact with an aluminum disk. Measurements of local velocity and of temperature distributions are presented as well as longitudinal turbulence profiles. The mean temperature profiles were measured through thermocouples.

An experimental investigation on flow structure and heat transfer from a single round jet impinging perpendicularly on a flat plate has been performed by Hofmann et al. [22]. Heat transfer has been studied by means of thermography.

Fig. 1 Experimental arrangement for PIV investigation [24]



The influence of nozzle-to-plate distance and Reynolds number on local heat transfer coefficient has been investigated.

Jet impingement heat transfer from a round gas jet to a flat wall was investigated numerically for a ratio of two between the jet inlet to wall distance by Vincent and Walther [23]. The jet Reynolds number used was 1.66×10^5 and the temperature difference between jet inlet and impingement wall was 1600 K. They did not include in their investigation the thermal radiation. A considerable influence of the turbulence intensity at the jet inlet was observed in the stagnation region. The choice of turbulence model also influenced the heat transfer predictions significantly.

Based on a review of the literature, there is a paucity of information concerning the experimental and numerical simulation of turbulent impinging plane jet with large h/e ratios over a smooth flat surface. Moreover, there is an increasing number of practical applications in which the value of h/e is large. Therefore, it is of interest to examine this factor on the evolution of impinging jet. In this study, the second order model (RSM) was carried out for different nozzle-to-plate spacing ($h/e = 14$ and 28) at a Reynolds number $Re = 3000$. The experiments performed using a Particle Image Velocimetry technique (PIV) have been used as the benchmark to validate the numerical model and for examining the influence of this parameter on the impinging jet evolution.

2 Experimental study

A plane jet of air impinging on a heated smooth flat surface is produced by the apparatus shown in Fig. 1. The jet emerged from a plane nozzle (3 mm wide and 42 mm length). The surface was made of copper, of dimensions $210 \times 170 \times 8$ mm³. It is located at a distance h from the nozzle. The position of the plate can be varied to provide nozzle-to-plate distances between 14 and 28 nozzle widths. Experimental results were obtained for jet Reynolds number equal to 3000. It is based on the centerline velocity at the nozzle exit v_j and the slot nozzle width e . The temperature is uniform and well distributed along the entire plate. Furthermore, we have used eight thermocouples, which are integrated and regularly spaced along the impact surface. In addition, to limit reflection of laser sheet closing to the plate, the plate is painted with matte black paint.

The jet is seeded with glycerin particles whose diameter is approximately equivalent to 1 μm (the seeding density $\cong 30$ particles ml⁻¹ of pure jet fluid) (Fig. 1). As its name suggests, the PIV technique records the position over time of small tracer particles introduced into the flow to extract the local fluid velocity. All the velocity measurements were made using the PIV technique. The velocity fields were measured using the single-frame double-exposure PIV method. This technique is performed with a TSI Power View system, including a 50 Mj dual YAG laser

which produces two flat pulses, the duration of one ranging from 5×10^{-9} to 10^{-8} s, a Power View 4 Mhigh resolution cross-correlation camera ($2 \text{ k} \times 2 \text{ k}$ resolution, 12 bits), a synchronizer and “Insight” Windows-based software for acquisition, processing and post-processing. The time delay between two pulses depends on the mean flow velocity and for our case, the time delay is $70 \mu\text{s}$. The light scattered by the seeded particles is recorded with CCD camera. The camera records 2 frames that are separated in time by the time interval dt which is the time interval between the laser pulses. The images were transferred to the control computer. Then the local displacement vector for the images of the particles is determined by mean of cross-correlation method. The final fields were averaged by means of 200 successive acquisitions. For each point, experimental uncertainties are estimated with the following criterion: $\frac{V_{\max} - V_{\min}}{V_{\text{av}}}$ where V_{\max} , V_{\min} , and V_{av} , respectively are the maximum velocity, the minimum velocity, and the average velocity measured during all the process. The uncertainties were about 5 %. This process is repeated for all interrogation areas of the PIV image [24].

3 Numerical simulations

3.1 Governing equations

The experimental geometric and dynamic conditions result in the generation of a three-dimensional, steady and turbulent flow. It is characterized by the dimensionless Reynolds number equivalent to 3000. The simulation of the problem requires the resolution of the conservation laws of mass, momentum and energy. In the Cartesian coordinate system, the equations governing this problem are obtained using the Reynolds decomposition and are thus written in the following form:

$$\frac{\partial(\bar{\rho} \bar{u}_i)}{\partial x_i} = 0 \quad (1)$$

$$\frac{\partial(\bar{\rho} \bar{u}_j \bar{u}_i)}{\partial x_j} = -\frac{\partial \bar{p}}{\partial x_i} + \frac{\partial}{\partial x_j} \left(\mu \frac{\partial \bar{u}_i}{\partial x_j} - \overline{\rho u'_i u'_j} \right) + (\bar{\rho}_{\infty} - \bar{\rho}) g \delta_{ij} \quad (2)$$

$$\frac{\partial(\bar{\rho} \bar{u}_j \bar{T})}{\partial x_j} = \frac{\partial}{\partial x_j} \left[\left(\frac{\mu}{\text{Pr}} + \frac{\mu_t}{\sigma_t} \right) \frac{\partial \bar{T}}{\partial x_j} \right] \quad (3)$$

u_i, T and x_i are the mean velocity, the temperature and the coordinate in the i direction, respectively. P represents the mean pressure. Theoretical analysis and prediction of turbulence requires the use of a turbulence closure model. In

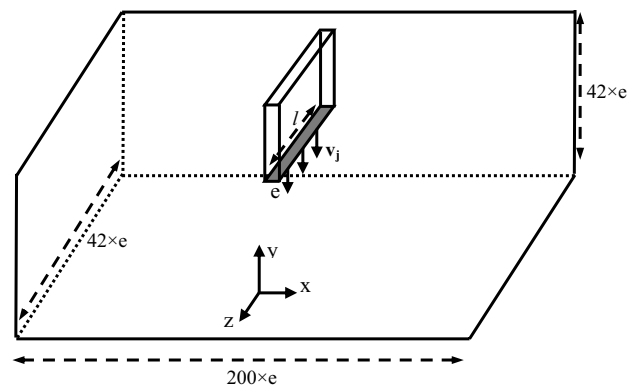


Fig. 2 Schematic of the model geometry

this study, computations were performed with a second-order turbulence model (RSM).

The following equation is solved:

$$\underbrace{\frac{\partial}{\partial x_k} (\bar{\rho} \bar{u}_k \bar{u}'_i \bar{u}'_j)}_{C_{ij}} = \underbrace{\frac{\partial}{\partial x_k} \mu \frac{\partial}{\partial x_k} (\bar{u}'_i \bar{u}'_j)}_{D_{ij}^T} - \rho \underbrace{\left[\bar{u}'_i \bar{u}'_k \frac{\partial \bar{u}_j}{\partial x_k} + \bar{u}'_j \bar{u}'_k \frac{\partial \bar{u}_i}{\partial x_k} \right]}_{P_{ij}} + D_{ij}^T + G_{ij} + \phi_{ij} + \varepsilon_{ij} \quad (4)$$

Where the symbols C_{ij} , D_{ij}^T , D_{ij}^v , P_{ij} , G_{ij} , ϕ_{ij} and ε_{ij} denote, respectively, the convective term, the turbulent diffusion, the viscous diffusion, the stress production, the buoyancy production, the pressure strain and the dissipation term [25].

The equation of the turbulent kinetic energy (k) and that of the dissipation rate of the kinetic energy (ε) which are relative to the second-order model are defined as follows:

$$\frac{\partial(\bar{\rho} \bar{u}_j k)}{\partial x_j} = \frac{\partial}{\partial x_j} \left[\mu + \frac{\mu_t}{\sigma_k} \frac{\partial k}{\partial x_j} \right] + \frac{1}{2} (P_{ii} + G_{ii}) - \bar{\rho} \varepsilon \quad (5)$$

$$\frac{\partial(\bar{\rho} \bar{u}_j \varepsilon)}{\partial x_j} = \frac{\partial}{\partial x_j} \left[\mu + \frac{\mu_t}{\sigma_\varepsilon} \frac{\partial \varepsilon}{\partial x_j} \right] + C_{\varepsilon 1} \frac{1}{2} \frac{\varepsilon}{k} P_{ii} - C_{\varepsilon 2} \frac{\bar{\rho} \varepsilon^2}{k} \quad (6)$$

The empirical constants that appear in the above equations are given by the following values: $C_{\varepsilon 1} = 1.44$, $C_{\varepsilon 2} = 1.92$, $\sigma_k = 0.82$ and $\sigma_\varepsilon = 1.0$ [26].

3.2 Flow configuration and boundary conditions

The geometrical configuration is presented in Fig. 2. The jet is emitted from a nozzle of rectangular section ($l \times e = 42 \times 3 \text{ mm}^2$). The Reynolds number based on the nozzle width was 3000. Two different distances between

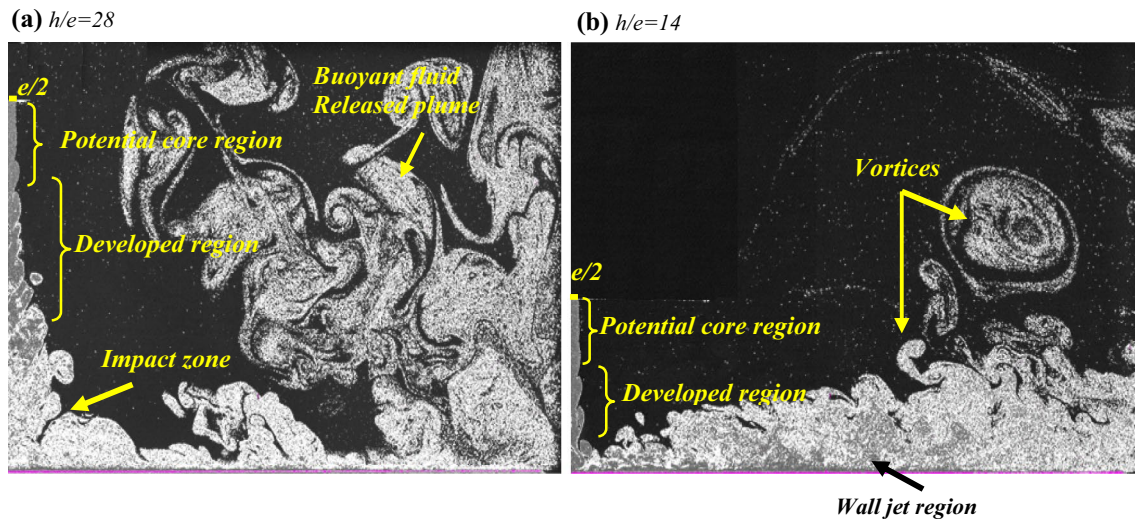


Fig. 3 Instantaneous visualization of the flow in the symmetry plane for $Re = 3000$ and $T_p = 54\text{ }^\circ\text{C}$

the nozzle exit and the flat plate “ h/e ” are examined in this study: 14 and 28. The computational domain is $200e \times 42e \times 42e$ in the longitudinal (x), vertical (y), and lateral (z) directions, respectively.

The boundary conditions for the flow field simulation are specified as follows. The mean jet velocity is v_j and with a ambient temperature ($T_a = 22\text{ }^\circ\text{C}$). A turbulence intensity of 5.8 % is imposed by the experience. Wall functions are performed on the impingement plate with zero roughness and non-slip condition. The impingement plate is at a temperature T_p , of $54\text{ }^\circ\text{C}$.

The wall function approach is based on two regional near-wall flow division [27]; the viscous and log-law sub-layer. The use of wall functions requires that the first grid point adjacent to the wall is within the logarithmic region: $30 < y^+ < 100$ and most preferable, however, is the lower limit: $y^+ = 30$. At outlet, along the x and z directions, the boundary zero gradients in the normal direction are prescribed.

3.3 Numerical method

The resolution of the aforementioned governing equations conditions is carried out using the finite volume method (FVM). This method allows the discretization of these equations using the first-order upwind interpolation scheme. The pressure velocity coupling is achieved through the SIMPLE algorithm [28]. The elimination method of Gauss associated with an under-relaxation technique is used to solve the resulting tridiagonal matrix.

To describe the behavior of the global flow particularly dynamics and heat transfer variation induced by the impinging air jet on a heated flat plate, we adopted a fine

mesh in zones where interesting interactions take place. The mesh system was non-uniform, highly refined near the jet nozzle. The interaction region where the jet impact the target was very complicated that is why the grid layout near this flat surface was specified to be much finer than that in the downstream region.

4 Results and discussion

Figure 3 gives an overall view of the mean flow field in terms of nozzle-to-impingement-plate distance, obtained for $Re = 3000$ and for a heated plate ($T_p = 54\text{ }^\circ\text{C}$) as determined from the PIV techniques. The flow field of an impinging jet divided into three regions: Firstly, there is the free jet region; this region is divided also to two zones: The first zone is called the potential core zone, where the centerline velocity is equal to the nozzle outlet velocity and the turbulence intensity level is relatively low. After potential core disappeared, the jet fluid discharging from the nozzle is developed in the developing zone due to large penetration of the mass in strong shear layer. The jet shear layers also actively participate in the entrainment of ambient fluid and in the growth of turbulent flow fluctuations. An oscillating flow is roll up to form vortices, which increase in size and strength with the axial distance. The variation of nozzle-to-plate distance has an effect on the expansion of the flow, it became less strong with increasing jet-to plate separation ($h/e = 28$). As jet the approaches the plate, a flow field is characterized by an impingement zone. The impinging jet shows very complicated flow phenomena inside the stagnation zone also known as the impact zone, due to interaction between the air jet and the solid impingement plate,

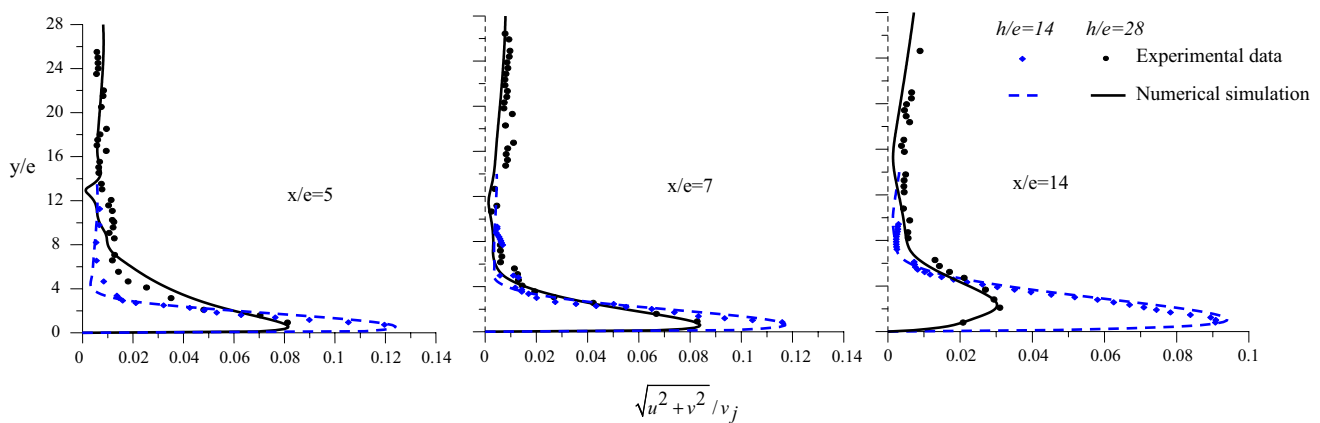


Fig. 4 Effect of nozzle-to-plate distances on the evolution of the mean velocity magnitude for $Re = 3000$ and $T_p = 54\text{ }^\circ\text{C}$

consisting of a reflection and sudden change of flow direction toward the radial direction from the stagnation point. The preservation of the coherent vortices in this zone is a strong function of jet-to-surface spacing. These vortices appear to be smaller in this zone for a small h/e . Further, from the axis jet, the flow enters a wall jet region where the flow moves laterally outward parallel to the wall. The impact of the distance between the jet exit and the plate is remarked. For a lesser jet-to-surface separation, the wall jet exhibits higher levels of turbulence. A boundary layer between the plate and the fluid is also formed, and as the flow develops downstream, both the mixing shear layer and the boundary layer grow. In contrast, the re-entrainment of buoyant fluid by the wall jet became progressively weaker for a smaller h/e ($h/e = 14$). The vertically rising plume flow is well established and more developed for a higher nozzle-to-plate spacing than the other case ($h/e = 14$). This features performed the heat transfer between the heated plate and the global flow.

In Fig. 4, we analyzed the influence of the height between the nozzle and the plate on the development of the mean velocity magnitude at three different longitudinal locations ($x/e = 5$, $x/e = 7$ and $x/e = 14$) and for the Reynolds number equal to $Re = 3000$. Comparison with our experimental data for different position show excellent agreement near the wall particularly in terms of the location and magnitude of the maximum velocity. For $x/e = 5$, the mean velocity magnitude is important showing the entrainment of the air jet caused by the presence of the heat plate. A peak in the mean velocities magnitude appears near the wall (at normal position $y/e = 2$) due to the large pressure gradient originating from the stagnation point. The maximum value decreases with increasing h/e because the flow of this case may have a lower boundary layer thickness with a slightly higher degree of turbulence. The maximum of velocity magnitude is found at longitudinal station $x/e = 7$. This maximum is only just below the

mean axial velocity at the jet exit. Going further longitudinally for $x/e = 14$, the peak of the mean velocity magnitude decreases because the air jet loses energy in the wall region and the velocity profile is widened in spatially. The mean velocity magnitude, for a larger distance between nozzle-to-plate $h/e = 28$, decay is faster near the plate and thus more efficient turbulent mixing is required.

Figure 5 displayed the effect of jet to plate spacing on the evolution of the dimensionless turbulent kinetic energy along the vertical coordinate (y/e) and at different longitudinal locations ($x/e = 5$, $x/e = 7$ and $x/e = 14$). The kinetic energy distributions, for different nozzle to-plate spacing and for different longitudinal positions, especially near the wall, show a very good agreement between the numerical simulation and the measured data. Near the stagnation zone ($x/e = 5$), the turbulent kinetic energy passes through a maximum near the wall around the vertical position $y/e = 2$. The highest levels of k/v_j^2 are found for the greater nozzle to plate spacing due to the presence of the shear layer between the jet and the ambient air. Further downstream at the longitudinal stations $x/e = 7$ and $x/e = 14$, the entrainment of the air jet into the wall jet region has resulted in a loss of flow kinetic energy and may cause a lower transfer rate. The effect of different jet-to-target plate distances persist along the wall jet region. It is concluded, therefore, for larger wall to-jet spacing (over 28 jet nozzle width), the turbulence kinetic energy increases as the distance from the exit jet, y/e , is decreased, reaches a peak near the wall. Thereafter the magnitude of peak value appears to be slightly lower than the other case.

The influence of nozzle-plate distance on the evolution of the Reynolds stress $\overline{u'v'}/v_j^2$ is shown in Fig. 6. Overall, the Reynolds stress obtained from the RSM model exhibit good agreement with the data using PIV technique. The behavior of the Reynolds stress near the centerline, $x/e = 5$, slowly increases towards the wall reaching a peak value of normal coordinate $y/e = 0.15$. For the case

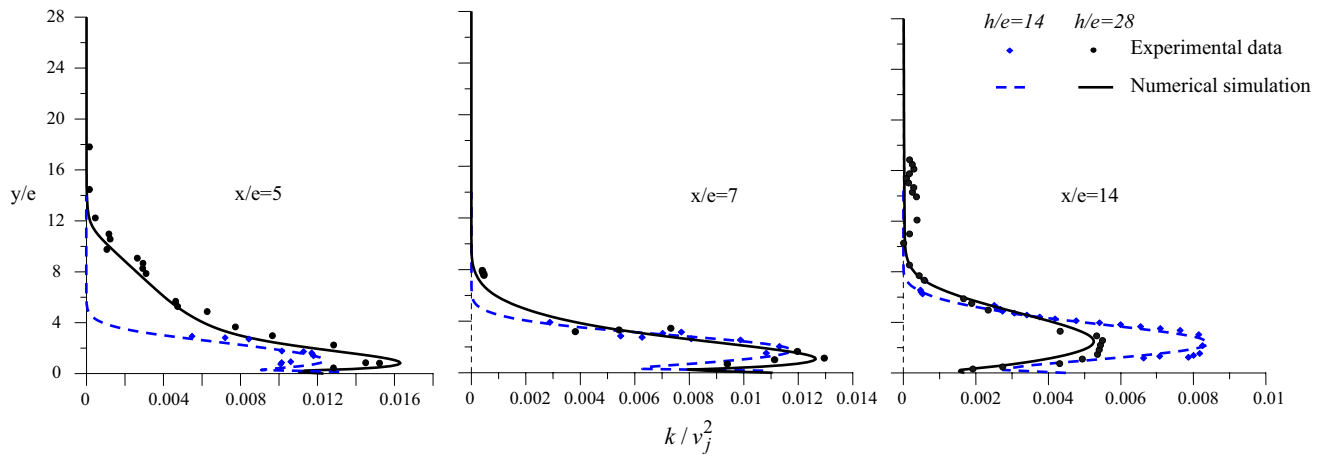


Fig. 5 Effect of nozzle-to-plate distances on the evolution of the turbulent kinetic energy for $Re = 3000$ and $T_p = 54\text{ }^\circ\text{C}$

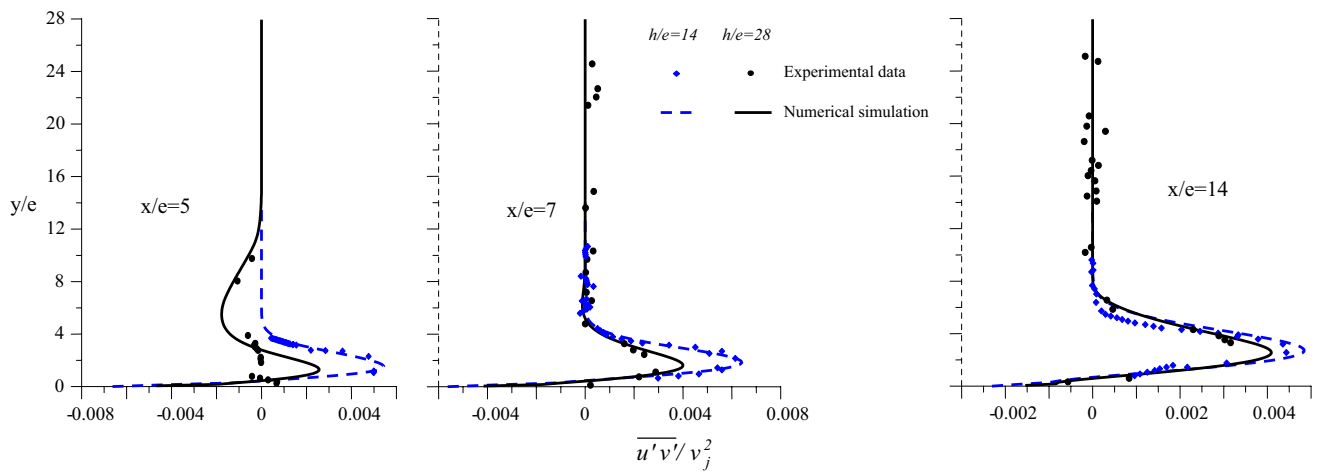


Fig. 6 Effect of nozzle-to-plate distance on the evolution of the Reynolds shear stress $\overline{u'v'}/v_j^2$ for $Re = 3000$ and $T_p = 54\text{ }^\circ\text{C}$

$h/e = 14$, $\overline{u'v'}/v_j^2$ has a sharp rise near the wall exceeding that of the case $h/e = 28$. It should be noted the presence of a negative levels of Reynolds stress for nozzle –plate distance $h/e = 28$. This value are found at the vertical station $y/e = 5$, due to the presence of the shear layer between the jet and the ambient air. As one moves away from the axis jet, an increase of the Reynolds stress near the wall (which occurs also for two cases of nozzle-plate distance $h/e = 14$ and $h/e = 28$) arises from the shear induced by the flow acceleration away from the stagnation point. The figure shows that the fluctuating velocities decrease with increasing the nozzle-to-plate spacing ($h/e = 28$). The decrease of the fluctuating velocity components simply reflects that the fluid in this zone passes through a more dynamic part of the turbulent mixing layer. Going further from the stagnation zone, $x/e = 14$, the streamlines of the flow

are approximately parallel to the wall and there is a very marked reduction in turbulence intensity. Thus, the shear weakens gradually further downstream and the turbulence intensity takes on an almost uniform level in the wall jet.

The present part is concerned in the wall shear stress and wall pressure distributions produced on the plane surface while reviewing the influence of nozzle –to-plate distance h/e . The wall shear stress and the wall pressure distribution are dimensionalised by ρv_j^2 where v_j is the jet exit velocity and ρ is the air density. Figure 7 depicts the wall shear stress distribution for fully developed jet impingement for different jet-to target separation ($h/e = 14$ and $h/e = 28$). Based on this analysis, it appears that the magnitude of the shear stress increases when moving away from the axis jet and there is a peak which occurs near the stagnation zone at longitudinal station $x/e = 10$. The evolution of the wall

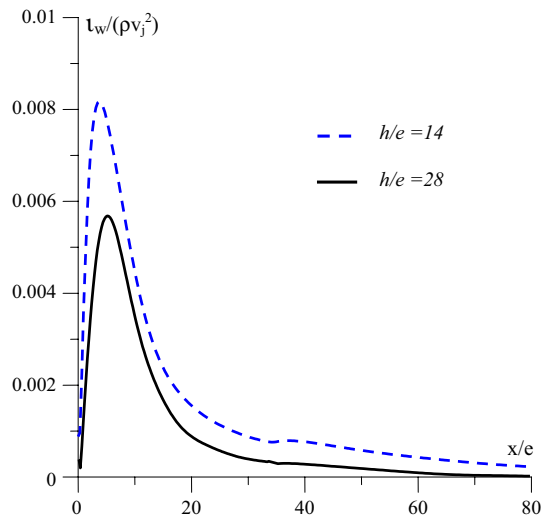


Fig. 7 The wall shear stress distributions for different nozzle-to-plate distances h/e for $Re = 3000$ and $T_p = 54\text{ }^\circ\text{C}$

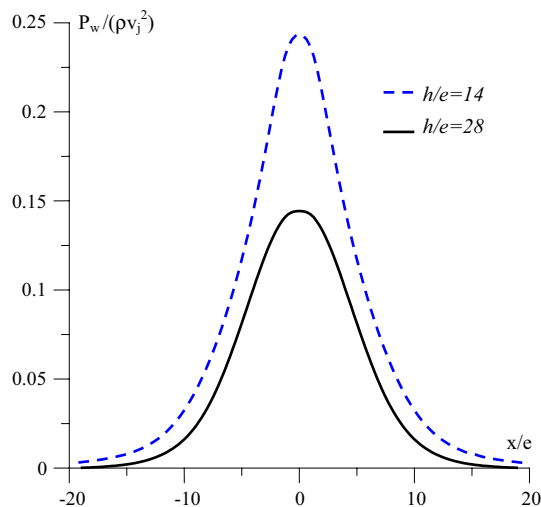


Fig. 8 Wall pressure distributions for different nozzle-to-plate distances h/e for $Re = 3000$ and $T_p = 54\text{ }^\circ\text{C}$

shear stress is considerably affected by the higher jet-plate distance $h/e = 28$. As observed, the peak value appears to be greatly shorter under this later jet height. This is consistent with the observation of Alekseenko and Markovich [29] that the wall shear stress is more pronounced for lower jet heights, which exhibit lower free-stream turbulence levels near the stagnation zone. Therefore, this feature gives rise to increase the wall friction and the heat transfer rate.

The distribution of the dimensionless wall pressure distributions according to the dimensionless axial coordinate (x/e) and under the effect of the distance nozzle -to- plate distance is presented in Fig. 8. The figure clearly reveals that the maximum pressure occurs at the stagnation point

($x/e = 0$) for the all nozzle-to-plate spacing is studied and it decreases with increase in longitudinal direction x/e . The observed distribution of the mean pressure exhibits a bell-shaped Gaussian profile at the $-2.5 < x/e < 2.5$ zone, with a peak pressure at the stagnation point ($x/e = 0$). This feature of the pressure profile is reported by many others example Tu et al. [31] and Beltaos et al. [30]. Furthermore, the wall pressure distribution was found to be sensitive to the nozzle-to-plate spacing. At low separation distance ($h/e = 14$), the stagnation pressure, at the position $x/e = 0$, is rather larger than the other spacing, due to rapidly decreasing of axial velocity in the deflection zone.

Finally, we proceeded to the elaboration of the thermal fields at various nozzle to-plate spacing. The dimensional temperature distribution $\theta = \frac{T - T_a}{T_p - T_a}$ in the flow is shown in Fig. 9. This figure clearly reveals that the distribution of the temperature have similar behavior for the different nozzle-to-plate spacing; they are decomposed into two parts, the first part with sharp slopes away from the plate corresponds on the abrupt reduction of the temperature. The second part characterized by a much more gradual slope near the plate, is distinguished by a slower decay until the stabilization of the temperature is attained. Generally, we observed that the temperature distribution is slightly affected by the variation of the nozzle to-plate spacing. For $x/e = 0$, and for a greater nozzle-to-impingement plate distance ($h/e = 28$), There is an important thermal transfer of the flow field near the heated plate. Near of the jet centerline ($x/e = 5$ and $x/e = 7$) and for a short nozzle-to-impingement plate distance ($h/e = 14$), the temperature of the fluid becomes greater. However, farther along the jet axis ($x/e = 14$ and $x/e = 21$), the temperature of the fluid obtained for larger plate separations ($h/e = 28$) becomes smaller than in the case for $h/e = 14$, owing to the presence of the vertically rising plume flow.

5 Conclusion

A numerical simulation model has been performed to investigate the dynamical and turbulent aspect of a turbulent air jet impinging on a heated plate. These results are compared with our experimental data. The experimental technique is that of a non-intrusive measurement of particle image velocimetry (PIV). According to the results, the second order turbulence closure model (RSM) gives a good agreement with experimental data. The results show that the flow field is affected by varying the nozzle to-plate spacing ($h/e = 14$ and $h/e = 28$). For a turbulent air jet ($Re = 3000$), the influence of the distance between the nozzle exit and the flat plate on the evolution of the mean velocity and on the turbulent fluctuation is remarked. The nozzle-to-plate spacing has a strong influence on the flow

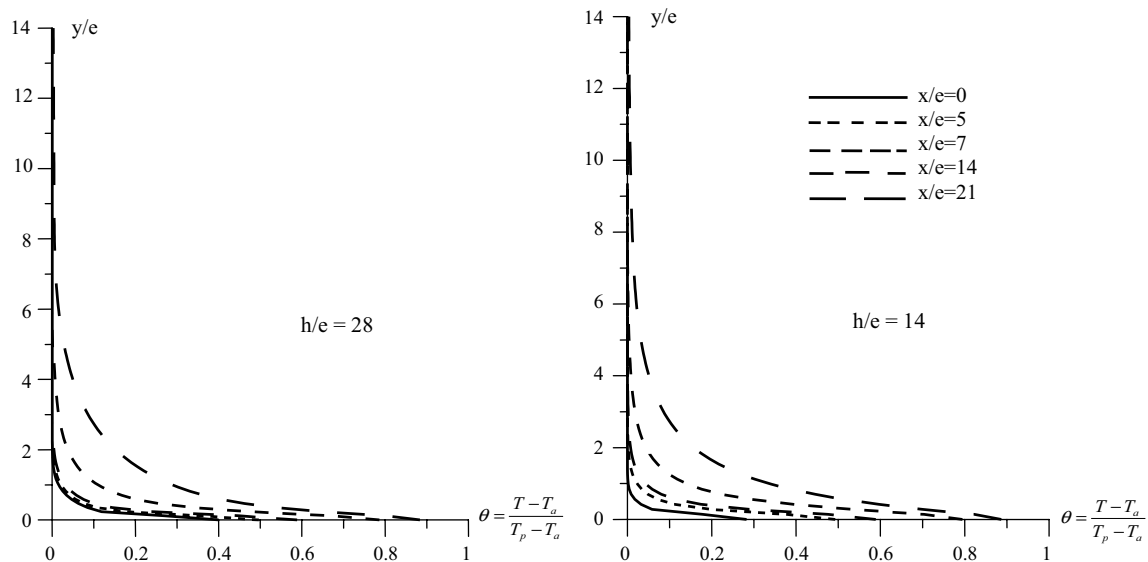


Fig. 9 Effect of nozzle-to-plate distance on the evolution of the temperature for $Re = 3000$ and $T_p = 54\text{ }^\circ\text{C}$

character, both within the vertical jet and within the wall jet region. For the smaller spacing, the mean velocity and turbulence measurements become important and the wall heat transfer becomes high. In addition, the wall shear stress and the wall pressure is found depending on the nozzle-to-surface spacing (h/e). The wall shear stress distribution and the wall pressure are more pronounced for lower jet heights. Therefore, this feature gives rise to increase the wall friction and the heat transfer rate.

References

- Martin H (1977) Heat and mass transfer between impinging gas jets and solid surface. *Adv Heat Transf* 13:1–60
- Hollworth BR, Durbin M (1992) Impingement cooling of electronics. *ASME J Heat Transf* 114:607–613
- Viskanta R (1993) Heat transfer to impinging isothermal gas and flame jets. *Exp Therm Fluid Sci* 6(1):111–134
- Polat S, Huang B, Majumdar AS, Douglas WJM (1989) Numerical flow and heat transfer under impinging jets: a review. *Annu Rev Numer Fluid Mech Heat Transf* 2:157–197
- Lytel D, Webb BW (1994) Air jet impingement heat transfer at low nozzle-plate spacings. *Int J Heat Mass Transf* 37:1687–1697
- Rundström D, Moshfegh B (2008) Investigation of heat transfer and pressure drop of an impinging jet in a cross-flow for cooling of a heated cube. *J Heat Transf-Trans ASME* 130 (12)
- Choo KS, Kim SJ (2010) Heat transfer characteristics of impinging air jets under a fixed pumping power condition. *Int J Heat Mass Transf* 53:320–326
- Li HL, Chiang HW, Hsu CN (2011) Jet impingement and forced convection cooling experimental study in rotating turbine blades. *Int J Turbo Jet-Engines* 28:147–158
- Masip Y, Rivas A, Larraona GS, Anton R, Ramos JC, Moshfegh B (2012) Experimental study of the turbulent flow around a single wall-mounted cube exposed to a cross-flow and an impinging jet. *Int J Heat Fluid Flow* 38:50–71
- Polat S, Huang B, Majumdar AB, Douglas WJM (1989) Numerical flow and heat transfer under impinging jets: a review. In: Tien CL (ed) *Annual review of numerical fluid mechanics and heat transfer*. Hemisphere Publishing Corporation, Washington
- Gutmark E, Wolfshtein M, Wygnanski I (1978) The plane turbulent impinging jet. *J Fluid Mech* 88(4):737–756
- Cooper D, Jackson DC, Launder BE, Liao GX (1993) Impingement jet studies for turbulence model assessment—I. Flow-field experiments. *Int J Heat Mass Transf* 36(10):2675–2684
- Knowles K, Mysko M (1998) Turbulence measurements in radial wall-jets. *Exp Thermal Fluid Sci* 17(1–2):71–78
- O’Donovan TS, Murray DB (2007) Jet impingement heat transfer—Part I: mean and root-mean-square heat transfer and velocity distributions. *Int J Heat Mass Transf* 50(17–18):3291–3301
- Baughn JWB, Shimizu S (1989) Heat transfer measurements from a surface with uniform heat flux and an impinging jet. *ASME. J Heat Transf* 111:1096
- Narayanan V, Seyed-Yagoobi J, Page RH (2004) An experimental study of fluid mechanics and heat transfer in an impinging slot jet flow. *Int J Heat Mass Transf* 47(8–9):1827–1845
- Koseoglu MF, Baskaya S (2008) The effect of flow field and turbulence on heat transfer characteristics of confined circular and elliptic impinging jets. *Int J Therm Sci* 47:1332–1346
- Ben Kalifa R, Habli S, Mahjoub Saïd N, Bournot H, Le Palec G (2016) Parametric analysis of a round jet impingement on a heated plate. *Int J Heat Fluid Flow* 57:11–23
- Xu ZY, Hangan H (2008) Scale, boundary and inlet condition effects on impinging jets. *J Wind Eng Ind Aerodyn* 96(12):2383–2402
- Beaubert F, Viazzo S (2003) Large eddy simulations of plane turbulent impinging jets at moderate Reynolds numbers. *Int J Heat Fluid Flow* 24:512–519
- Guerra DR, Su J, Freire AP (2005) The near wall behavior of an impinging jet. *Int J Heat Mass Transf* 48:2829–2840
- Hofmann HM, Kind M, Martin H (2007) Measurements on steady state heat transfer and flow structure and new correlations for heat and mass transfer in submerged impinging jets. *Int J of Heat Mass Transf* 50:3957–3965
- Jensen MV, Walther JH (2013) Numerical analysis of jet impingement heat transfer at high jet Reynolds number and large

- temperature difference. *Heat Transf Eng.* doi:[10.1080/01457632.2012.746153](https://doi.org/10.1080/01457632.2012.746153)
24. Said NM, Mhiri H, Golli S, Le Palec G, Bournot Ph (2003) Three dimensional numerical calculations of a jet in external crossflow: application to pollutant dispersion. *J Heat Transf* 125:510–522
 25. Amamou A, Habli S, Saïd NM, Bournot P, Le Palec G (2015) Numerical study of turbulent round jet in a uniform counterflow using a second order Reynolds Stress Model. *J Hydro-environ Res* 9:482–495
 26. Wilcox DC (1998) Turbulence modeling for CFD. DCW Industries Inc, La Canada
 27. Daly BJ, Harlow FH (1970) Transport equations in turbulence. *Phys Fluids* 13:2634–2649
 28. Patankar SV, Spalding DB (1972) A calculation procedure for heat, mass and momentum transfer in three dimensional parabolic flows. *Int J Heat Mass Transf* 15:1787–1806
 29. Alekseenko SV, Markovich DM (1994) Electro-diffusion diagnostics of wall shear stresses in impinging jets. *J Appl Electrochem* 24:626–631
 30. Tu CV, Wood DH (1996) Wall pressure and shear stress measurements beneath an impinging jet. *Expl Therm Fluid Sci* 13:364–373
 31. Beltaos S, Rajaratnam N (1973) Plane turbulent impinging jets. *J Hydraulics Res* 11:29–59